# Interpreting the widespread nonlinear force spectra of intermolecular bonds

Raymond W. Friddle[a,b,1], Aleksandr Noy[c,d], and James J. De Yoreo[a,1]

[a]Molecular Foundry, Lawrence Berkeley National Laboratory, Berkeley, CA 94720; [b]Sandia National Laboratories, Livermore, CA 94550; [c]School of Natural Sciences, University of California, Merced, CA 95343; and [d]Physical and Life Sciences Directorate, Lawrence Livermore National Laboratory, Livermore, CA 94550

Edited by Steven M. Block, Stanford University, Stanford, CA, and approved July 3, 2012 (received for review February 21, 2012)

**Single molecule force spectroscopy probes the strength, lifetime, and energetic details of intermolecular interactions in a simple experiment. A growing number of these studies have reported distinctly nonlinear trends in rupture force with loading rate that are typically explained in conventional models by invoking complex escape pathways. Recent analyses suggested that these trends should be expected even for simple barriers based on the basic assumptions of bond rupture dynamics and thus may represent the norm rather than the exception. Here we explore how these nonlinear trends reflect the two fundamental regimes of bond rupture: (*i*) a near-equilibrium regime, produced either by bond reforming in the case of a single bond or by asynchronized rupture of multiple individual bonds, and (*ii*) a kinetic regime produced by fast, non-equilibrium bond rupture. We analyze both single- and multi-bonded cases, describe the full evolution of the system as it transitions between near- and far-from-equilibrium loading regimes, and show that both interpretations produce essentially identical force spectra. Data from 10 different molecular systems show that this model provides a comprehensive description of force spectra for a diverse suite of bonds over experimentally relevant loading rates, removes the inconsistencies of previous interpretations of transition state distances, and gives ready access to both kinetic and thermodynamic information about the interaction. These results imply that single-molecule binding free energies for a vast number of bonds have already been measured.**

single molecule mechanics | multivalency | nonequilibrium dynamics | free energy

Dynamic force spectroscopy (DFS) (1–3) provides researchers the ability to characterize the microscopic basis of inter- and intra-molecular bonding. The technique is rooted in the early works of Eyring (4, 5) and Zhurkov (6) where the failure times of stressed materials were explained through Arrhenius-like models of thermal activation over energy barriers. This microscopic view was scaled down further by Bell (7), and later Evans (3), to analyze the failure of single-molecule bonds under stress. Evans and coworkers found (3, 8) that the typical rupture force of a single bond varies as the logarithm of the loading rate, $f \sim \ln r$, when it is driven far from equilibrium, where $r = df/dt$ is the rate of increasing force with time. This model has served as a foundation for the modern analysis of force spectroscopy experiments, in which the data, arranged as a plot of the rupture force vs. log-loading rate (the force spectrum) are expected to form a straight line, at least for irreversible rupture of a single bond over a single energy barrier.

Although early works pointed out the consequences of reversibility and multiple bonds (8, 9), the irreversible single-bond model quickly became the standard for analyzing force spectra. Then, in a seminal experiment on the biotin-avidin system, more than one linear trend appeared in the force spectrum (2). Under the irreversible, linear model of single bond rupture, the logical conclusion was that these data were evidence of a succession of separate barriers along the rupture pathway. This interesting result seemed to support the remarkable strength of the biotin-avidin bond and appeared to reveal intermediates that were previously inaccessible experimentally. Surprisingly, as follow-up studies collected more data on a variety of different molecular systems, a peculiar commonality began to emerge from these experiments: Most showed nonlinear trends in the force spectra. Even a cursory search of the literature finds more than 55 publications that report nonlinear force spectra (see *SI Text* for details) and cover a large variety of intermolecular systems involving macromolecules (10), peptides (11), small molecules (12), inorganic probes and self-assembled monolayers (13), and binding in both aqueous and organic solvents (14).

A few exceptions notwithstanding, the vast majority of these studies interpreted the data as representing two barriers along the unbinding pathway. Thus the commonality of nonlinear force spectra suggests somewhat unnaturally that energy landscapes with well-resolved intermediate barriers, which might reasonably be expected in the case of complex macromolecules or high-affinity interactions, are instead widespread among all types of molecular species and experimental preparations. Moreover, a significant portion of those studies employing the two-barrier interpretation report a distance to the "inner" barrier that inexplicably—and nonphysically—fall orders of magnitude below 1 Å. These facts suggest that the common existence of two prominent barriers could be a misconception based on a false interpretation of these nonlinear trends, which instead capture some other aspects of the physics of bond rupture.

In this paper we present a self-consistent interpretation that accounts for the characteristic features of many—if not most—force spectroscopy experiments without invoking additional complexity to the escape pathway. We draw upon previous numerical and asymptotic analyses, which suggested that nonlinearity in force spectra arises either through the reforming of a single bond at slow loading rates (8, 9, 15) or as a consequence of asynchronous fluctuations of several independent interactions that comprise a multivalent or heterogeneous cluster (7, 8, 16–18). In either case the force spectrum passes through two primary regimes—an equilibrium regime characterized by a finite force and a kinetic regime characterized by a weak dependence on loading rate, $f \sim \ln r$. While these primary loading regimes have each been analyzed in detail (15–17), the lack of a tractable model spanning both regimes has excluded it as a competing theory to the multi-barrier model. Here we derive accurate interpolations between equilibrium and kinetic regimes in both the single- and multi-bond cases. Finally, we show that this approach accurately

Author contributions: R.W.F., A.N., and J.J.D.Y. designed research; R.W.F. performed research; R.W.F. analyzed data; and R.W.F., A.N., and J.J.D.Y. wrote the paper.

The authors declare no conflict of interest.

This article is a PNAS Direct Submission.

Freely available online through the PNAS open access option.

[1]To whom correspondence may be addressed. E-mail: jjdeyoreo@lbl.gov or rwfridd@sandia.gov.

This article contains supporting information online at www.pnas.org/lookup/suppl/doi:10.1073/pnas.1202946109/-/DCSupplemental.

describes a large number of nonlinear force spectra collected from vastly dissimilar intermolecular systems.

## Results and Discussion

We begin with the all-important single-bond system that illustrates the main physical assumptions of our model. Evans and Williams discussed the difficulties in measuring a true single-bond when blindly allowing molecules to connect between the probe and substrate (8). Their main conclusion was that, unless additional knowledge is used to determine bond valency (19), the actual experiment is more likely to measure multiple bonds than single bonds. Thus, we then follow with a description of the multiple bond case, because this is the most probable configuration measured in the laboratory. Finally, we compare the models with numerical simulations, our own experimental data, and 10 other datasets taken from the literature.

**Single Bond.** In a DFS experiment the force transducer [atomic force microscope (AFM) cantilever, biomembrane force probe, or an optical trap] typically exhibits a Hookean response to displacement, and thus if a single bond is characterized by a single barrier, the combined bond/transducer system comprises two states: the bound state, $b$, when the bond is formed, and the unbound state, $u$, when the bond is broken and the system fluctuates in the parabolic well of the transducer. If we assume that the time scale of intra-well relaxation is faster than any other time scales of the system, then the probability of finding the system in the bound state, $p_b(t)$, is described by the master equation of a two-state Markov process (8),

$$\frac{dp_b}{dt} = -k_u(t)p_b + k_b(t)p_u, \qquad [1]$$

where the instantaneous unbinding, $k_u(t)$, and binding, $k_b(t)$, rates are time-dependent to reflect their dependence on force.

The transition rates used in Eq. **1** must adequately describe the dynamics, yet they do not need to be complicated for modeling typical laboratory experiments. Several recent publications (20–23) showed that it is possible to produce nonlinearities in the force spectrum at very fast loading rates under an assumption of a force-dependent transition state (which can result from certain model-based potentials). However, the loading rate required to explore this regime of nonlinearity is 4 to 7 orders of magnitude greater than the upper end of loading rates reached in the laboratory (see *SI Text* for details). Therefore, for this work we chose to use the simpler unbinding rate given by the Bell model (7), which estimates the effect of force on the barrier to be linear and depends on a minimal number of parameters [Eq. **2**]. In this model, the rebinding rate is approximately the natural frequency of the transducer, $k_b^0$, scaled by the Boltzmann-weighted energy of a spring extended between the barrier location $x_t$ and the relative displacement of the spring minimum, $f/k_c$ (see Fig. 1*A*). Thus the unbinding and binding transition rates are given by,

$$k_u(f) = k_u^0 \exp\left[\beta\left(fx_t - \frac{1}{2}k_c x_t^2\right)\right], \qquad [2]$$

$$k_b(f) = k_b^0 \exp\left[-\beta\frac{k_c}{2}\left(\frac{f}{k_c} - x_t\right)^2\right] = k_u(f)\exp\left[\beta\left(\Delta G_{bu} - \frac{f^2}{2k_c}\right)\right], \qquad [3]$$

where $k_u^0$ is the intrinsic unbinding rate of the molecular complex (where the probe-molecule connection may contribute additional fluctuations and a modified damping), $\beta^{-1} = k_B T$ is Boltzmann's constant times the temperature, and $e^{\beta\Delta G_{bu}} = k_b^0/k_u^0$ defines the equilibrium free energy $\Delta G_{bu} = G_u - G_b$ of the bond $G_b$, relative to the free cantilever $G_u$.

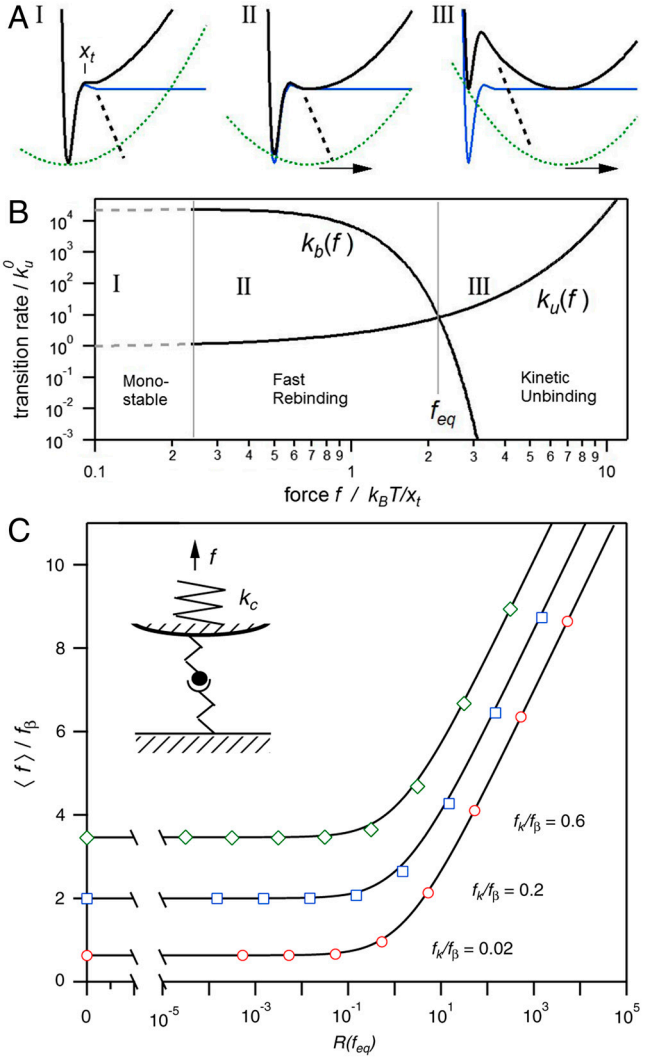


**Fig. 1.** Potential energy profile, two-state kinetics, and comparison of the single-bond model force spectrum to the two-state master equation. (*A*) 1D energy profile of a single bond (blue curve) loaded by a harmonic potential (dotted green curve). The total potential of the system is represented by the thick black curve. At zero load (I), the harmonic and bond potential minima coincide and a single stable minimum exists. As the harmonic potential is pulled beyond the bond barrier (II) a second minimum is created and the system becomes bistable; however, the barrier impeding rebinding is negligible. Pulling further (III) the re-entry barrier increases and significantly reduces the chance of rebinding. The black dashed line represents the pathway that is commonly assumed beyond the barrier. That is, once the system overcomes the barrier it is carried away irreversibly. (*B*) Transition rates for unbinding [Eq. **2**] and rebinding [Eq. **3**] using typical parameters of $k_u^0 = 0.1\ s^{-1}$, $x_t = 1$ Å, $\Delta G_{bu} = 10\,k_BT$, and $k_c = 100$ pN/nm. Rates are in units of $k_u^0$ and force is in units of $k_BT/x_t$. The regimes corresponding to stages in the upper panels are partitioned for comparison. (*C*) The differential equation defining the two-state master equation [Eq. **1**] is solved by numerical integration (symbols) with the Bulirsch-Stoer method using Richardson extrapolation (Igor Pro, Wavemetrics). Results are shown for $\Delta G_{bu} = 10\,k_BT$, and three different confinement force values $f_k = k_c x_t$, which govern the effects of the probing spring constant on the resulting spectrum. The single-bond model in Eq. **6** is calculated with identical parameters for comparison (solid curves).

The two rates in Eqs. **2** and **3** cross at a unique force, $f_{eq}$, given by (1, 24)

$$f_{eq} = \sqrt{2k_c\Delta G_{bu}}, \qquad [4]$$

which defines the equilibrium force for the bond/transducer system. It can also be shown that for $\beta\Delta G_{bu} \gg 1$ the mean force in

the limit of vanishing loading rate is also equal to $f_{eq}$. The existence of this limiting force—the lowest force required to break a bond for a given force transducer stiffness—has been predicted by a number of theoretical studies (8, 9, 15), and we have recently presented an experimental demonstration of this phenomenon (24). On a more fundamental level, the existence of this force reflects major differences between the dynamics of free bonds and bonds attached to a force probe that adds a confining potential to the system and creates a defined unbound state. Note that even polymer linkers between the molecule and the probe behave like an entropic spring over large fractional extensions when the contour length is significantly larger than the persistence length (25). This effect results in an effectively spring-like potential for small loads where near-equilibrium effects are important. The major underlying assumption of the linear first-passage model is that a free noncovalent bond will break on its own in absence of external force if left alone for a sufficiently long time. However, when the same bond is attached to a force transducer, the presence of the transducer potential precludes the bond from breaking until a minimal force is applied, at which point a second state is created. Given the existence of the two states, another profound consequence is that the overall dynamics of the system should now be dependent on the shape of the second well and thus on the transducer stiffness $k_c$ in all regimes of bond rupture (26–28).

Inspection of Eqs. **3** and **4** reveals that the rebinding rate can be expressed as a function of the unbinding rate and the equilibrium force $f_{eq}$. Surprisingly, in this case the complete two-state process described by Eq. **1** includes only one additional free parameter, $f_{eq}$, to the usual unknowns $k_u^0$, and $x_t$. To understand the significance of $f_{eq}$ consider the evolution of the transition rates with force (Fig. 1*B*). For forces less than $f_{eq}$ the rebinding rate dominates the dynamics, acting to keep the system in the bound state. At forces beyond $f_{eq}$ the rebinding rate falls off rapidly due to the quadratic term $-f^2/2k_c$ in the exponent, leaving the unbinding rate as the only significant contributor to the dynamics. Note that, although the distribution of rupture forces extends below $f_{eq}$, it is impossible to observe a mean force below $f_{eq}$. This important feature of the bond rupture process allows us to simplify the two-state master equation (Eq. **1**) by starting the bond loading process at $f = f_{eq}$, instead of starting at $f = 0$ [Seifert (15) used the same approach for analyzing the two-state problem through a mean-field approach]. With this simplification we truncate Eq. **1** to,

$$\int_1^{p_b} \frac{dp_b'}{p_b'} \cong -\frac{1}{r}\int_{f_{eq}}^{f} k_u(f')df' \qquad [5]$$

and inserting Eq. **2** in Eq. **5** we find the mean rupture force $\langle f\rangle$,

$$\langle f\rangle = f_{eq} + f_\beta e^{\frac{1}{R(f_{eq})}} E_1\left(\frac{1}{R(f_{eq})}\right), \qquad R(f_{eq}) = \frac{r}{k_u(f_{eq})f_\beta}, \qquad [6]$$

where $f_\beta = k_B T/x_t$ is the thermal force scale, and $E_1(z) = \int_z^\infty \frac{e^{-s}}{s} ds$ is the exponential integral. We can also produce an analytical approximation to Eq. **6** by using the relationship $e^z E_1(z) \cong \ln(1 + e^{-\gamma}/z)$, where $\gamma = 0.577...$ is Euler's constant. The most significant feature of Eq. **6** is that it extends over the two primary regimes of the single-bond dynamic force spectrum: a linear regime in the slow loading limit, $\langle f\rangle_{r\to 0} = f_{eq} + r/k_u(f_{eq})$, and a nonlinear regime in the fast loading limit, $\langle f\rangle_{r\to\infty} = f_\beta \ln(e^{-\gamma}R(0))$, leading to the characteristic $\ln r$ dependence expected for the irreversible rupture of single bonds. Indeed Eq. **6** is remarkably accurate: If we compare its predictions with the numerical solution of Eq. **1** we see negligible differences over a variety of parameters and loading rates (Fig. 1*C*), with the largest error of roughly 5% occurring at the "elbow" of the spectrum where $R(f_{eq}) \sim 1$.

**Multiple Bonds.** We now turn to the system that comprises $N$ bonds arranged in parallel between the probe and substrate. As we discussed in the introduction, this is arguably the common state of affairs in the laboratory (8). In a continuum approach, the number of formed parallel bonds $N_b$, of which $N_t$ total bonds are allowed to independently unbind and rebind, is represented by the differential equation (7, 16–18)

$$r\frac{dN_b}{df} = -N_b k_u(f/N_b) + (N_t - N_b)k_a, \qquad [7]$$

where $k_u(f)$ is given by Eq. **2** and $k_a$ is the constant rebinding rate of an individual molecule acting over a short distance from its retracted position while the overall cluster remains bound. This multiple bond model has been extensively examined numerically and by asymptotic analysis (7, 16–18, 29–31). Again, just as with the single bond case, two primary regimes emerge. At slow loading rates, fluctuations in the number of closed bonds is relatively fast (Fig. 2), and the system establishes a meta-stable number of bonds, $N(f) = N_t/(1 + k_u(f/N)/k_a)$. From here we define $N$ as the equilibrated number of formed bonds at zero force,

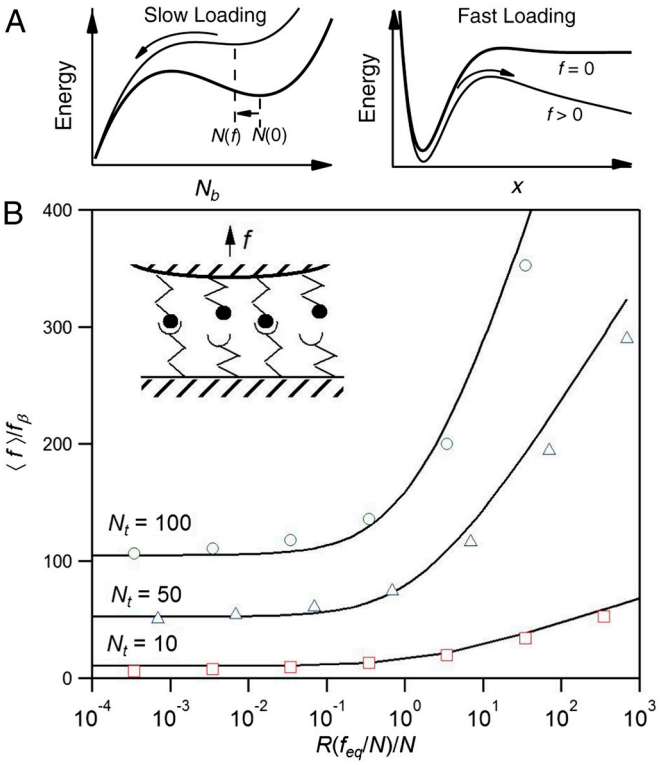


**Fig. 2.** The multi-bond model and comparison to Monte Carlo simulation of $N$-bonded systems. (*A*) Schematics of the two limiting pathways when several bonds are allowed to independently unbind and rebind, which are dictated by loading rate. At slow loading, the motion along the $N_b$ coordinate is relatively slow, and rupture occurs once $N_b$ diffusively crosses a threshold defined by a maximum in the free energy (18, 30). At fast loading, the force is quickly raised and thus the drop in $N_b$ will be fast after the initial bond ruptures. In this case the spatial diffusion of one bond over its energy barrier is the slow process which dictates rupture of the cluster. (*B*) The mean rupture force for the indicated number of $N_t$ bonds, as described by Eq. **7**, is solved by the Gillespie algorithm for $k_a/k_u^0 = 10$. Rupture forces for a given trajectory are determined when $N_b = 0$, and hundreds of trajectories are used to produce the mean rupture force (symbols) plotted here against the dimensionless loading rate. For comparison, the multi-bond model in Eq. **9** is calculated (solid curves) for the same ratio of transition rates, and with $N = N_t/(1 + k_u^0/k_a)$.

$N = N_t/(1 + k_u^0/k_a)$. Stability of the cluster is completely lost when the force exceeds the equilibrium force (7, 17, 30)

$$f_{\text{eq}} = Nf_\beta W(e^{\beta\Delta G_{ba}-1}), \quad [8]$$

where $W(x)$ is the Lambert $W$-function, which is defined as the solution for $W$ to the equation $We^W = x$, and $e^{\beta\Delta G_{ba}} = k_a/k_u^0$ defines the equilibrium free energy $\Delta G_{ba} = G_a - G_b$ of the closed bond $G_b$ relative to an open bond $G_a$ within the bound cluster. In systems where fluctuations in $N_b$ are large, rupture can occur long before stability in $N$ is lost, leading to a more gradual decrease in rupture force with decreasing loading rate than predicted here. The second primary regime appears at fast loading rates where the rebinding rate $k_a$, and hence fluctuations in $N_b$, become less important. Here the force reaches higher loads and the bonds rupture rapidly after the first bond fails, leading to the irreversible rupture force, $\langle f\rangle_N \sim Nf_\beta \ln(r/k_u^0 f_\beta N)$ (16, 17). Note that the force spectrum in this regime follows the same classic $f \sim \ln r$ trend, therefore the resulting force spectrum will look qualitatively very similar to the single bond case. We obtain an interpolation between these two regimes (see *SI Text* for details):

$$\langle f\rangle_N \cong f_{\text{eq}} + Nf_\beta e^{\frac{N}{R(f_{\text{eq}}/N)}} E_1\left(\frac{N}{R(f_{\text{eq}}/N)}\right),$$
$$R(f_{\text{eq}}/N) = \frac{r}{k_u(f_{\text{eq}}/N)f_\beta}. \quad [9]$$

Again, this equation is remarkably accurate in describing the force spectrum over the complete range of loading rates. When we compared the spectrum predicted by Eq. **9** to Monte Carlo simulation of the complete model in Eq. **7** over seven decades in loading rate (Fig. 2) using the Gillespie algorithm (32), we found that this model accurately captured the two primary trends, as well as the crossover region between the two loading rate regimes.

Interestingly, the multi-bond model of Eq. **9** shows that, if we combine the number of bonds $N$ into an apparent force scale,

$$f_\beta^{\text{app}} \equiv Nf_\beta = \frac{k_B T}{x_t/N}, \quad [10]$$

along with a generic definition of an equilibrium force $f_{\text{eq}}$, then the multi-bond force spectrum takes the same mathematical form as the single-bond model in Eq. **6**. Eq. **10** shows that the multiple-bond model modifies the single-bond model simply through the parameter $N$, which factors inversely to the transition state $x_t$ everywhere in the function. Significantly, this observation explains the unreasonably small transition state distances reported in many force spectroscopy experiments. When an $N$-bonded system is analyzed in the kinetic regime using the common-practice single-bond model, the fitted apparent transition state, $x_t^{\text{app}} = x_t/N$, will be $N$ times smaller than the true distance $x_t$.

**Comparison to Experimental Data.** These models provide a theoretical basis for extracting a consistent set of interaction parameters of a bond over the broader context of loading conditions, not just those that satisfy the far-from-equilibrium condition. To test the validity of our model experimentally, we measured rupture forces for the nickel-mediated bond between nitrilotriacetic acid (NTA) and poly-Histidine ($His_6$) over four decades of loading rates (see *SI Text*). As Fig. 3*A* demonstrates, the mean force with log-loading-rate displays the expected two-regime behavior. The fit of Eq. **6** to the data is excellent, and we obtain reasonable values for all parameters: $x_t = 0.92 \pm 0.15$ Å, and $k_u^0 = 4.31 \pm 4.23$ s$^{-1}$. The kinetic unbinding rate of 4.3 s$^{-1}$ is of the same order as $1.8 \pm 0.40$ s$^{-1}$ found for a single Ni-NTA unbinding from $His_6$ by time-

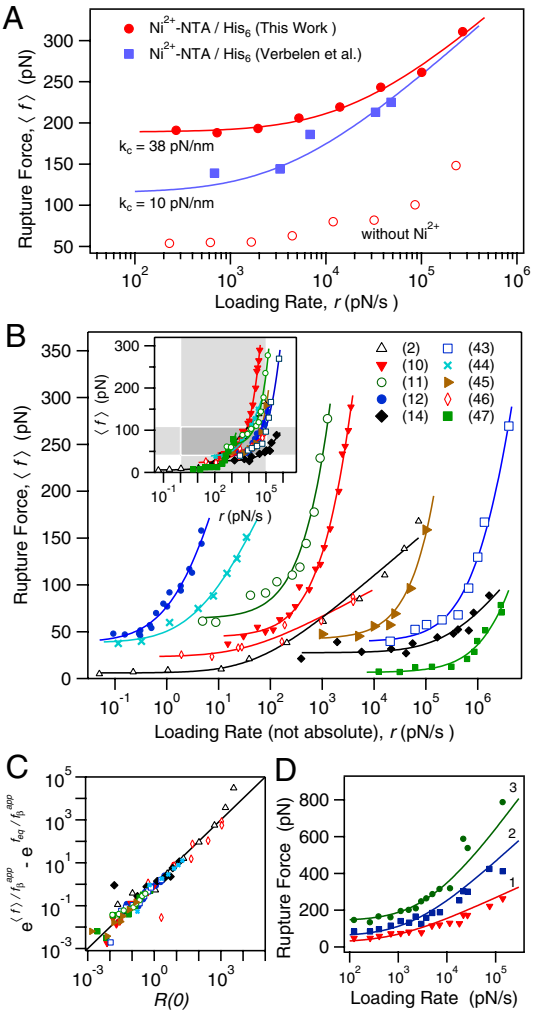


**Fig. 3.** Model fits to the nonlinear force spectra of intermolecular bonds. (*A*) Force spectrum of the Ni-NTA/$His_6$ bond measured in this work along with the data of Verbelen et al. (34). Measurements made without $Ni^{2+}$ demonstrate the specificity of the interaction (open circles). Solid lines represent fits to Eq. **6** using identical parameters for both data sets except for the respective spring constants. (*B*) Force spectra of 10 data sets taken from the literature are fit to Eq. **9** assuming a generic equilibrium force and apparent transition state distance. Data are exploded along the loading rate axis for clarity. Inset: The same force spectra in their raw form illustrating the theoretical range of equilibrium force and cross-over loading rate span (shaded regions). The upward inflection at high forces in the Biotin/Avidin data of ref. 2 may be due to limited sampling rate effects (41) and enhanced force error at very fast loading rates (42). (*C*) The same data in *B* plotted in the natural coordinates of Eq. **9** (see Eq. **S3**) show that all spectra collapse onto a single line. (*D*) Biotin-avidin bond rupture data of Teulon et al. (35) are globally fitted to Eq. **9** assuming $N = 1$, 2, and 3 parallel bonds. Only $f_{\text{eq}}$ is independently fit, while $x_t$ and $k_u^0$ are shared. Fitted values are $x_t = 0.78$ Å, $k_u^0 = 6.75$ s$^{-1}$, and $f_{\text{eq}} = 24.6$ pN ($N = 1$), 58.5 pN ($N = 2$), 142.3 pN ($N = 3$). Legend in (*B*) refers to references and corresponding bonds as follows: Biotin/Avidin (2); LFA-1/ICAM-1 [rest 3A9] (10); A$\beta$-40/A$\beta$-40 (11); N,C,N-pincer/pyridine (12); $Si_3N_4$/Mica in Ethanol (14); peptide/steel (43); Integrin/Fibronectin (44; Lysozyme/Anti-Lysozyme (45); Dig/Anti-Dig (46); Actomyosin/ADP (47).

resolved fluorescence (33). The same system was previously investigated by another group (34), with the only difference that the probe-surface linkages of $His_6$ and NTA functionalities were inverted. Those measurements (Fig. 3*A*) appear to diverge from ours. Attempts to corroborate the two data sets using the multi-bond model, through varying $N$, were unsuccessful. However, when we replace the value for the spring constant in our experiments (38 pN/nm) with that used in the previous study

**Table 1. Fitted parameters of the reversible and irreversible theories to literature data**

| Bond (Ref.) | Reversible model* | | | Irreversible model* | |
|---|---|---|---|---|---|
| | $f_{eq}$(pN) | $x_t^{app}$(Å) | $k_u^0$($s^{-1}$) | $x_t^{inner}/x_t^{outer}$(Å) | $k_u^{inner}/k_u^{outer}$($s^{-1}$) |
| $His_6$/Ni-NTA (this work) | 189 ± 3.5 | 0.92 ± 0.15 | 4.18 ± 4.14 | — / — | — / — |
| Lysozyme/Anti-Lysozyme (45) | 42 ± 8.0 | 0.05 ± 0.07 | 753 ± 168 | 0.06 / 10.0 | 150 / 0.001 |
| Biotin/Avidin† (2) | 6.1 ± 5.1 | 3.10 ± 0.17 | 0.75 ± 0.24 | 3.0 / 30.0 | — / — |
| N,C,N-Pincer/Pyridine‡ (12) | 38.5 ± 4.8 | 0.36 ± 0.13 | 368.0 ± 143 | — / — | 81 / — |
| Digoxigenin/Anti-Digoxigenin (46) | 23.2 ± 4.9 | 3.18 ± 0.66 | 4.37 ± 4.34 | 3.5 / 11.5 | 4.56 / 0.015 |
| LFA-1/ICAM-1 (10) | 44.2 ± 3.1 | 0.09 ± 0.02 | 101.4 ± 12.1 | 0.18 / 1.5 | 57 / 4 |
| Integrin-Fibronectin: α5β1/FN7-10 (44) | 38.2 ± 3.6 | 0.73 ± 0.14 | 32.5 ± 12.3 | 0.95 / 3.65 | 25 / 0.85 |
| $Si_3N_4$/Mica [in EtOH] (14) | 27.6 ± 3.3 | 1.21 ± 0.68 | 917.4 ± 909 | 1.43 / 11.65 | — / — |
| peptide/steel (43) | 39.4 ± 6.3 | 0.15 ± 0.05 | 1034 ± 252 | 0.46 / 4.3 | 340 / 4.2 |
| Actomyosin/ADP (47) | 6.5 ± 2.6 | 0.25 ± 0.18 | 12.3 ± 3.4 | 1.0 / 26.0 | 4.4 / 0.02 |
| Amyloid dimer: Aβ-40/Aβ-40 (11) | 63.8 ± 6.0 | 0.05 ± 0.05 | 439 ± 128 | 0.3 / 2.6 | 111 / 0.88 |

*_Reversible model_ values are ±1 S.D. and obtained using Eq. **9**. _Irreversible model_ values are the published parameters from fitting each linear segment piece-wise.

†Merkel et al. (2) divided the force spectrum into four segments, mapping barriers at 1.2, 3, 5, and 30 Å. Shown here are parameters for the two dominant segments.

‡Kersey et al. (12) do not apply the double-barrier interpretation. They offer several possible sources for the low-force regime, one of which is rebinding.

(10 pN/nm) and use exactly the same parameters obtained from our data, the force spectrum predicted by the single-bond model of Eq. **6** provides an excellent fit to these data points. This result highlights the significance of the transducer stiffness on the resulting force spectrum (9, 24, 26, 27) and demonstrates that proper analysis can unify the force spectra collected under different experimental conditions.

The deeper implications of the model in Eq. **9** become clearer when we apply it to DFS data for a wide range of systems. In addition to our data, we have compiled force spectra from 10 different studies, each probing a different intermolecular bond and extending over a sufficient span of loading rates to exhibit the two dynamic regimes. Eq. **9** fits the full range of all data sets very well, even for those datasets in which the lowest value of the pulling rate is still too large to fully reach the plateau of the near-equilibrium regime (Fig. 3; see also Table 1 for the fitted parameter values). Moreover, all data collapse onto a single universal line when plotted using the natural coordinates of that equation (Fig. 3*C*; and see Eq. **S3**). We also compare our model to the outstanding analysis of DFS measurements for multiples of biotin-avidin bonds by Teulon et al. (35). To be valid, the parameters predicted by Eq. **9** should remain constant regardless of the number of bonds, $N$. In Fig. 3*D* we present global fits to the three curves of Teulon et al. (assuming $N = 1$, 2, and 3, and keeping $x_t$ and $k_u^0$ unchanged for all datasets) and find good agreement with the data for all three curves.

As predicted by the multiple bond analysis, a number of spectra we examined produce apparent transition state distances that are unrealistically small, for example $6.3 \times 10^{-4}$ Å, $1.3 \times 10^{-3}$ Å, $1.5 \times 10^{-2}$ Å, and $1.4 \times 10^{-2}$ Å from refs. 13 and 36–38, respectively, with several on the order of $10^{-2}$ Å (see Table S1 for complete list of parameters). Note that these values are very similar to those given in the original publications using the linear $f \sim \ln r$ model on the high-force regime. Potential of mean force calculations generally find the distance from the minimum to the primary barrier to be on the order of 1 Å (39). With this rough estimate the apparent distances found on the order of $x_t^{app} = x_t/N \sim 10^{-2}$ Å reflect bond numbers around $N = 100$, which is the same number of bonds predicted when assuming thiol monolayers on Au-coated probes with 100 nm tip radii using JKR contact mechanics (40). We note that if our model is to be used to extract true transition state distances from experimental data from a multi-bond system, the number of bonds will need to be determined independently. Alternatively, independent methods of ensuring that measurements probe only single bond interactions (8) can be used prior to applying the single-bond model to the data. However, the intrinsic unbinding rate of a single bond $k_u^0$, and the single-bond free energy between the bound and closely unbound states $\Delta G_{ba}$, can both be determined without knowledge of $N$. Further discussion of the correlation between equilibrium force and transition state as it applies to bond valency is provided in *SI Text* (see Fig. S1).

What other arguments support or refute our interpretation? It is logical to assume that if rebinding plays a significant role in the bond rupture at slow loading rates then we should be able to observe these events in the raw data. However, this is not a trivial phenomenon to observe, because the rare sojourns in the unbound state may not be long enough to be observed with typical sampling rates on the order of 1 kHz. Hence fast sampling rates should be used at slow loading rates to confirm or discard near-equilibrium effects. In the multi-bonded scenario the question regarding rebinding events becomes irrelevant, because macroscopic rebinding from the completely unbound state is not required to establish the quasi-steady-state number of bonds and therefore the equilibrium force.

Finally, we consider the conditions required to observe nonlinearity within this model—that is, the loading rate that marks the crossover between near-equilibrium to kinetic regimes. Inspection of Figs. 1 and 2 shows—as a consequence of the exponential integral appearing in Eq. **9**—a useful relationship for benchmarking where this crossover occurs is when $R(f_{eq}/N)/N = 1$, or,

$$r_x = N f_\beta k_u (f_{eq}/N). \quad [11]$$

Using the extremes of experimentally observed values for $f_{eq} \sim 10$–200 pN, $k_u^0 \sim .01$–100 Hz, with nominal $x_t \sim 1$ Å and $N \sim 1$–50, we find crossover loading rates encompass a range $r_x \sim 1$–$10^5$ pN/s. Remarkably, this range brackets the typical loading rates explored in a laboratory, as shown by the shaded area in the inset to Fig. 3*B*. Likewise, we show in *SI Text* that the theoretical equilibrium unbinding force for a single-bond falls in the range of $f_{eq} \sim 40$ to 108 pN. Not only is this range above the noise limits of widely used AFM systems, but these forces can be quite high, and are remarkably consistent with the experimentally measured low-force regime data (see inset to Fig. 3*B*).

## Conclusions

The findings presented in this work raise the general question of whether the multi-barrier model is an appropriate interpretation of force spectroscopy experiments. Unfortunately, the multi-barrier model imposes any arbitrary number of barriers along the bond potential to match the number of linear trends observed in the experimental force spectrum. If fitting is the only criterion, then the multi-barrier hypothesis can never be rejected, because

this segmented approach can be tailored to fit any force spectrum. Further, it introduces at least twice as many free parameters as the number of perceived linear trends. In contrast, the single-barrier model presented here is based on a simpler potential energy surface, is governed by only three free parameters, and provides tangible, testable requirements, such as the cross-over loading rate and equilibrium force, that can be calculated based on physical parameters and compared against experiment. Thus, while the validity of a multi-barrier model is difficult to prove or disprove, researchers can easily test whether the data behave according to the predictions of the complete single-barrier model. Nonetheless, while the model presented here provides a comprehensive description of forced bonds comprising single-barrier interactions, we emphasize that experimental data not accounted for by such a description can arise for any number of reasons. It is up to the researcher to determine whether such deviations from the single-barrier description are an experimental artifact or a signature of a more complex energy landscape.

Our findings imply that both near- and far-from-equilibrium regimes are readily accessible in a DFS measurement, and these regimes are both inherent and ubiquitous. The results also show that, in most force spectroscopy experiments, multiple connections between the probe and surface cannot be treated simply as an effective correlated single bond, because conformational freedom in these systems permits microscopic unbinding between closely situated intermolecular pairs, establishing the equilibrium threshold for rupture. More importantly, if we abandon the assumption of strictly irreversible bond rupture inherent in the standard analysis, we find that both kinetic and equilibrium properties can be determined from a single dataset and the bond can be described by just three parameters: the transition state distance, the unbinding rate, and the value of $f_{eq}$. The surprising consequence of this conclusion is that the data required for determining equilibrium free energies corresponding to single- and multiple-bond scenarios are already available in the literature for a large number of intermolecular systems.

**ACKNOWLEDGMENTS.** This work was supported by the Office of Science, Office of Basic Energy Sciences of the U.S. Department of Energy under Contract DE-AC52-07NA27344. Measurements were performed at the Molecular Foundry, Lawrence Berkeley National Laboratory, with support from the Office of Science, Office of Basic Energy Sciences of the U.S. Department of Energy under Contract DE-AC02-05CH1123. Sandia is a multiprogram laboratory operated by Sandia Corporation, a Lockheed Martin Company, for the United States Department of Energy under contract DE-AC04-94AL85000. Work at Lawrence Livermore National Laboratory was performed under the auspices of the U.S. Department of Energy by under Contract DE-AC52-07NA27344.

1. Evans E (1998) Energy landscapes of biomolecular adhesion and receptor anchoring at interfaces explored with dynamic force spectroscopy. *Faraday Discuss* 111:1–16.
2. Merkel R, Nassoy P, Leung A, Ritchie K, Evans E (1999) Energy landscapes of receptor-ligand bonds explored with dynamic force spectroscopy. *Nature* 397:50–53.
3. Evans E, Ritchie K (1997) Dynamic strength of molecular adhesion bonds. *Biophys J* 72:1541–1555.
4. Eyring H (1936) Viscosity, plasticity, and diffusion as examples of absolute reaction rates. *J Chem Phys* 4:283–291.
5. Tobolsky A, Eyring H (1943) Mechanical properties of polymeric materials. *J Chem Phys* 11:125–134.
6. Zhurkov S (1965) Kinetic concept of the strength solids. *Int J FractMech* 1:311–322.
7. Bell G (1978) Models for the specific adhesion of cells to cells. *Science* 200:618–627.
8. Evans E, Williams P (2002) Les Houches—Ecole d'Ete de Physique Theorique. *Physics of Bio-molecules and Cells*, eds F Flyvbjerg, F Jülicher, P Ormos, and F David (Springer, Berlin, Heidelberg), Vol. 75, pp 145–204.
9. Evans E (2001) Probing the relation between force-lifetime-and chemistry in single molecular bonds. *Ann Rev Biophys Biomol Struct* 30:105–128.
10. Zhang X, Wojcikiewicz E, Moy VT (2002) Force spectroscopy of the leukocyte function-associated antigen-1/intercellular adhesion molecule-1 interaction. *Biophys J* 83:2270–2279.
11. Kim B-H, et al. (2011) Single-molecule atomic force microscopy force spectroscopy study of A$\beta$-40 interactions. *Biochemistry* 50:5154–5162.
12. Kersey FR, Loveless DM, Craig SL (2007) A hybrid polymer gel with controlled rates of cross-link rupture and self-repair. *J R Soc Interface* 4:373–380.
13. Ptak A, Gojzewski H, Kappl M, Butt H-J (2010) Quantitative analysis of the interaction between an atomic force microscopy tip and a hydrophobic monolayer. *J Phys Chem C* 114:21572–21578.
14. Zepeda S, Yeh Y, Noy A (2003) Determination of energy barriers for intermolecular interactions by variable temperature dynamic force spectroscopy. *Langmuir* 19:1457–1461.
15. Seifert U (2002) Dynamic strength of adhesion molecules: Role of rebinding and self-consistent rates. *Europhys Lett* 58:792–798.
16. Seifert U (2000) Rupture of multiple parallel molecular bonds under dynamic loading. *Phys Rev Lett* 84:2750–2753.
17. Erdmann T, Schwarz US (2004) Adhesion clusters under shared linear loading: A stochastic analysis. *Europhys Lett* 66:603–609.
18. Liang H-H, Chen H-Y (2011) Strength of adhesion clusters under shared linear loading. *Phys Rev E* 83:061914–061920.
19. Sulchek TA, et al. (2005) Dynamic force spectroscopy of parallel individual Mucin1-antibody bonds. *Proc Natl Acad Sci USA* 102:16638–16643.
20. Hummer G, Szabo A (2003) Kinetics from nonequilibrium single-molecule pulling experiments. *Biophys J* 85:5–15.
21. Dudko OK, Hummer G, Szabo A (2006) Intrinsic rates and activation free energies from single-molecule pulling experiments. *Phys Rev Lett* 96:108101–108104.
22. Lin H-J, Chen H-Y, Sheng Y-J, Tsao H-K (2007) Bell's expression and the generalized garg form for forced dissociation of a biomolecular complex. *Phys Rev Lett* 98:1–4.
23. Friddle RW (2008) Unified model of dynamic forced barrier crossing in single molecules. *Phys Rev Lett* 100:138302–138305.
24. Friddle R, Podsiadlo P, Artyukhin A, Noy A (2008) Near-equilibrium chemical force microscopy. *J Phys Chem C* 112:4986–4990.
25. Blundell JR, Terentjev EM (2007) Forces and extensions in semiflexible and rigid polymer chains and filaments. *J Phys A* 40:10951–10964.
26. Tshiprut Z, Klafter J, Urbakh M (2008) Single-molecule pulling experiments: When the stiffness of the pulling device matters. *Biophys J* 95:L42–L44.
27. Walton EB, Lee S, Van Vliet KJ (2008) Extending Bell's model: How force transducer stiffness alters measured unbinding forces and kinetics of molecular complexes. *Biophys J* 94:2621–2630.
28. Maitra A, Arya G (2010) Model accounting for the effects of pulling-device stiffness in the analyses of single-molecule force measurements. *Phys Rev Lett* 104:108301–108304.
29. Williams PM (2003) Analytical descriptions of dynamic force spectroscopy: Behaviour of multiple connections. *Anal Chim Acta* 479:107–115.
30. Lin H-J, Chen H-Y, Sheng Y-J, Tsao H-K (2010) Free energy and critical force for adhesion clusters. *Phys Rev E* 81:061908–061913.
31. Selhuber-Unkel C, et al. (2010) Cell adhesion strength is controlled by intermolecular spacing of adhesion receptors. *Biophys J* 98:543–551.
32. Gillespie DT (1977) Exact stochastic simulation of coupled chemical reactions. *J Phys Chem* 81:2340–2361.
33. Lata S, Reichel A, Brock R, Tampé R, Piehler J (2005) High-affinity adaptors for switchable recognition of histidine-tagged proteins. *J Am Chem Soc* 127:10205–10215.
34. Verbelen C, Gruber HJ, Dufre YF (2007) The NTA-$His_6$ bond is strong enough for AFM single-molecular recognition studies. *J Mol Recognit* 20:490–494.
35. Teulon J-M, et al. (2011) Single and multiple bonds in (strept)avidin-biotin interactions. *J Mol Recognit* 24:490–502.
36. Ptak A, Makowski M, Cichomski M (2010) Characterization of nanoscale adhesion between a fluoroalkyl silane monolayer and a silicon AFM tip. Complex character of the interaction potential. *Chem Phys Lett* 489:54–58.
37. Xu L-C, Siedlecki CA (2009) Atomic force microscopy studies of the initial interactions between fibrinogen and surfaces. *Langmuir* 25:3675–3681.
38. Sisquella X, et al. (2010) A single-molecule force spectroscopy nanosensor for the identification of new antibiotics and antimalarials. *FASEB J* 24:4203–4217.
39. Pettitt BM, Karplus M (1985) The potential of mean force between polyatomic molecules in polar molecular solvents. *J Chem Phys* 83:781–789.
40. Noy A, Vezenov DV, Lieber CM (1997) Chemical force microscopy. *Annu Rev Mater Sci* 27:381–421.
41. Li N, Guo S, Akhremitchev BB (2010) Apparent dependence of rupture force on loading rate in single-molecule force spectroscopy. *Chemphyschem* 11:2096–2098.
42. Perret E, Leung A, Feracci H, Evans E (2004) Trans-bonded pairs of E-cadherin exhibit a remarkable hierarchy of mechanical strengths. *Proc Natl Acad Sci USA* 101:16472–16477.
43. Landoulsi J, Dupres V (2011) Probing peptide-inorganic surface interaction at the single molecule level using force spectroscopy. *Chemphyschem* 12:1310–1316.
44. Li F, Redick SD, Erickson HP, Moy VT (2003) Force measurements of the alpha5beta1 integrin-fibronectin interaction. *Biophys J* 84:1252–1262.
45. Berquand A, et al. (2005) Antigen binding forces of single antilysozyme Fv fragments explored by atomic force microscopy. *Langmuir* 21:5517–5523.
46. Neuert G, Albrecht C, Pamir E, Gaub HE (2006) Dynamic force spectroscopy of the digoxigenin-antibody complex. *FEBS Lett* 580:505–509.
47. Guo B, Guilford WH (2006) Mechanics of actomyosin bonds in different nucleotide states are tuned to muscle contraction. *Proc Natl Acad Sci USA* 103:9844–9849.

# Corrections

## DEVELOPMENTAL BIOLOGY

Correction for "Neighbor of Brca1 gene (Nbr1) functions as a negative regulator of postnatal osteoblastic bone formation and p38 MAPK activity," by Caroline A. Whitehouse, Sarah Waters, Katie Marchbank, Alan Horner, Neil W. A. McGowan, Jelena V. Jovanovic, Guilherme M. Xavier, Takeshi G. Kashima, Martyn T. Cobourne, Gareth O. Richards, Paul T. Sharpe, Tim M. Skerry, Agamemnon E. Grigoriadis, and Ellen Solomon, which appeared in issue 29, July 20, 2010, of *Proc Natl Acad Sci USA* (107:12913–12918; first published June 29, 2010; 10.1073/pnas.0913058107).

The authors note that Figure 4 appeared incorrectly. A well image was duplicated within panel *C*. The corrected figure and its legend appear below. This error does not affect the conclusions of the article.

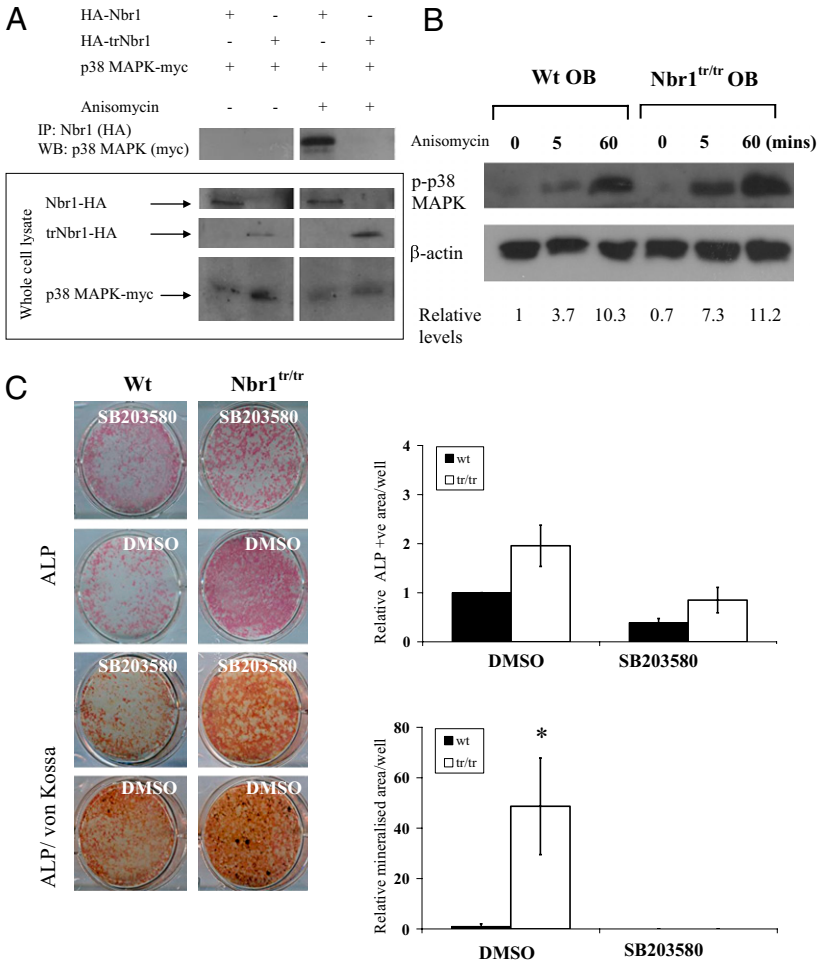


**Fig. 4.** p38 MAPK activity is increased in Nbr1$^{tr/tr}$ osteoblasts. (*A*) p-p38 MAPK interacts with full-length Nbr1 but not trNbr1. COS-7 cells were transfected with HA-Nbr1, HA-trNbr1, and p38 MAPKmyc constructs for 24 h and stimulated or not stimulated with 5 ng/mL anisomycin for 15 min; extracts were prepared, and co-immunoprecipitation of Nbr1 with p38 MAPK was detected by Western blot analysis. Representative blots of two experiments with similar results are shown. (*B*) Anisomycin-induced p38 MAPK activation in osteoblasts cultured from bone marrow of 3-mo-old Nbr1$^{tr/tr}$ mice is elevated and prolonged compared with Wt cells. (*C*) p38 MAPK inhibition rescues the increased differentiation phenotype in Nbr1$^{tr/tr}$ osteoblasts. Neonatal calvarial-derived osteoblast cultures from Wt or Nbr1$^{tr/tr}$ mice in osteogenic culture for 18 days in the presence of DMSO (vehicle) or 10 μM SB203580 were stained for alkaline phosphatase only [ALP (*Top two rows*)] or ALP followed by von Kossa [ALP/von Kossa (*Bottom two rows*)] and quantified using National Institutes of Health (NIH) Image software. The data represent the mean ± SD of triplicate representative wells normalized to untreated wild-type cells (*$P < 0.05$). Similar results were obtained in the presence of 0.1 μM SB203580.

www.pnas.org/cgi/doi/10.1073/pnas.1300714110

## BIOPHYSICS AND COMPUTATIONAL BIOLOGY, APPLIED PHYSICAL SCIENCES

Correction for "Interpreting the widespread nonlinear force spectra of intermolecular bonds," by Raymond W. Friddle, Aleksandr Noy, and James J. De Yoreo, which appeared in issue 34, August 21, 2012, of *Proc Natl Acad Sci USA* (109:13573–13578; first published August 6, 2012; 10.1073/pnas.1202946109).

The authors note that on page 13576, right column, first paragraph, line 8 "(38 pN/nm)" should instead appear as "(27 pN/nm)". The authors also note that Fig. 3 appeared incorrectly. The corrected figure and its legend appear below.

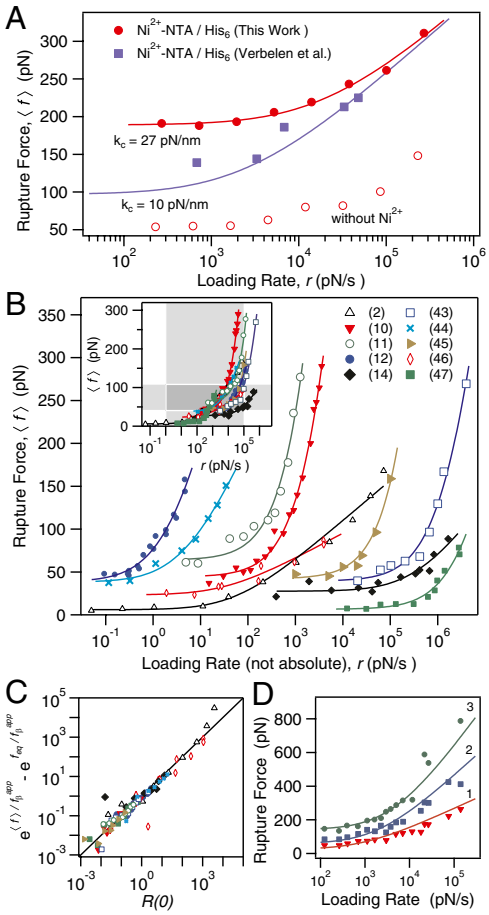


**Fig. 3.** Model fits to the nonlinear force spectra of intermolecular bonds. (*A*) Force spectrum of the Ni-NTA/His6 bond measured in this work along with the data of Verbelen et al. (34). Measurements made without $Ni^{2+}$ demonstrate the specificity of the interaction (open circles). Solid lines represent fits to Eq. 6 using identical parameters for both data sets except for the respective spring constants. (*B*) Force spectra of 10 data sets taken from the literature are fit to Eq. 9 assuming a generic equilibrium force and apparent transition state distance. Data are exploded along the loading rate axis for clarity. Inset: The same force spectra in their raw form illustrating the theoretical range of equilibrium force and cross-over loading rate span (shaded regions). The upward inflection at high forces in the Biotin/Avidin data of ref. 2 may be due to limited sampling rate effects (41) and enhanced force error at very fast loading rates (42). (*C*) The same data in *B* plotted in the natural coordinates of Eq. 9 (see Eq. S3) show that all spectra collapse onto a single line. (*D*) Biotin-avidin bond rupture data of Teulon et al. (35) are globally fitted to Eq. 9 assuming $N = 1$, 2, and 3 parallel bonds. Only $f_{eq}$ is independently fit, while $x_t$ and $k_u^0$ are shared. Fitted values are $x_t = 0.78$ Å, $k_u^0 = 6.75\ s^{-1}$, and $f_{eq} = 24.6$ pN ($N = 1$), 58.5 pN ($N = 2$), 142.3 pN ($N = 3$). Legend in (*B*) refers to references and corresponding bonds as follows: Biotin/Avidin (2); LFA-1/ICAM-1 [rest 3A9] (10); A$\beta$-40/A$\beta$-40 (11); N,C,N-pincer/pyridine (12); $Si_3N_4$/Mica in Ethanol (14); peptide/steel (43); Integrin/Fibronectin (44; Lysozyme/Anti-Lysozyme (45); Dig/Anti-Dig (46); Actomyosin/ADP (47).

www.pnas.org/cgi/doi/10.1073/pnas.1302149110

## MEDICAL SCIENCES

Correction for "Inflammasome-independent role of the apoptosis-associated speck-like protein containing CARD (ASC) in the adjuvant effect of MF59," by Ali H. Ellebedy, Christopher Lupfer, Hazem E. Ghoneim, Jennifer DeBeauchamp, Thirumala-Devi Kanneganti, and Richard J. Webby, which appeared in issue 7, February 15, 2011, of *Proc Natl Acad Sci USA* (108:2927–2932; first published January 26, 2011; 10.1073/pnas.1012455108).

The authors wish to note the following: "In Ellebedy et al. we showed a role for the apoptosis-associated speck-like protein containing CARD (ASC) in the adjuvant effect of MF59. However, in pilot studies in an alternative ASC-deficient mouse line generated by Dr. V. Dixit (Genentech, Inc.), this phenotype was not reproduced. A similar observation was recently reported, thus highlighting differences in the available ASC-deficient mouse lines (1). The data in Ellebedy et al. is accurate, and in that line of ASC-deficient mice there is indeed a reduced adjuvant effect of MF59. We stand by that data, but caution should be used in interpreting data gained from the different ASC-deficient mice."

1. Ippagunta SK, et al. (2012) Addendum: Defective Dock2 expression in a subset of ASC-deficient mouse lines. *Nat Immunol* 13(7):701–702.

www.pnas.org/cgi/doi/10.1073/pnas.1301192110

## NEUROSCIENCE

Correction for "D2 receptor overexpression in the striatum leads to a deficit in inhibitory transmission and dopamine sensitivity in mouse prefrontal cortex," by Yan-Chun Li, Christoph Kellendonk, Eleanor H. Simpson, Eric R. Kandel, and Wen-Jun Gao, which appeared in issue 29, July 19, 2011, of *Proc. Natl. Acad. Sci. USA* (108:12107-12112; first published July 5, 2011; 10.1073/pnas.1109718108).

The authors note that the National Institutes of Health grant number R01MH232395 should instead appear as R01MH085666.

www.pnas.org/cgi/doi/10.1073/pnas.1301683110